NeuroImage **11,** 359–369 (2000)
doi:10.1006/nimg.1999.0532, available online at http://www.idealibrary.com on IDEAL®

COMMENTS AND CONTROVERSIES

Theory of the Relation between Human Brain Activity (MEG) and Hand Movements

Armin Fuchs, Viktor K. Jirsa, and J. A. Scott Kelso

Center for Complex Systems and Brain Sciences, Florida Atlantic University, Boca Raton, Florida 33431

Received September 13, 1999

Earlier research established that spontaneous changes in human sensorimotor coordination are accompanied by qualitative changes in the spatiotemporal dynamics of neural activity measured by multisensor electroencephalography and magnetoencephalography. More recent research has demonstrated that a robust relation exists between brain activity and the movement profile produced. In particular, brain activity has been shown to correlate strongly with movement velocity independent of movement direction and mode of coordination. Using a recently developed field theoretical model of large-scale brain activity itself based on neuroanatomical and neurophysiological constraints we show here how these experimental findings relate to the field theory and how it is possible to reconstruct the movement profile via spatial and temporal integration of the brain signal. There is a unique relation between the quantities in the theory and the experimental data, and fit between the shape of the measured and the reconstructed time series for the movement is remarkably good given that there are no free parameters. © 2000 Academic Press

1. INTRODUCTION

Spontaneous changes in human coordination behavior have been a central research theme experimentally and theoretically for the past 2 decades (see for a review (Kelso, 1995; Haken, 1996). Recent developments in technology allow us to study the living brain noninvasively using behavioral coordination paradigms as a tool to prepare the brain in well-defined states. In the early 1990s it was shown that spontaneous changes in sensorimotor coordination are also accompanied by qualitative changes in the spatiotemporal dynamics of neural activity measured by multisensor magnetoencephalography (MEG) and electroencephalography (EEG) (Fuchs *et al.,* 1992; Jirsa *et al.,* 1995; Kelso *et al.,* 1992; Wallenstein *et al.,* 1995). More recently, a neurobiologically motivated theory which combines features of excitatory and inhibitory neural ensembles including their intra- and corticocortical connections was able to account for the observed relationship between brain activity and behavior for two different coordination paradigms (Jirsa and Haken, 1996, 1997; Jirsa *et al.,* 1998). Key features of this field theoretical approach describing neural activity as a function of space and time are the specific form of interaction within the neural mass and particular functional input or output units. The latter correspond to specific locations in the cortical sheet where, e.g., input from sensory pathways arrives driving the spatiotemporal dynamics. Likewise, cortical activity in motor-related areas can be used to drive muscle joint linkages external to the sheet. These functional anatomical units provide a bridge between internal dynamics of the cortex and the externally observed behavior. Here we show through a development of this theory how it is possible to directly connect cortical activity and kinematic properties of behavior. Specifically, we derive an equation from the field theory that can serve as a model in which signals emanating from the motor cortex are seen to drive the finger as a damped harmonic oscillator. This model reproduces the recently observed robust relationship between brain activity and velocity of movement (Kelso *et al.,* 1998).

In section 2 we summarize the recent experimental results by Kelso *et al.* demonstrating the correlation between brain activity and the movement profile. Section 3 describes the spatiotemporal decomposition techniques that were used to establish the foregoing relation. These methods serve as a necessary basis for connecting theory and experiment in section 4 in which we reconstruct the observed relation between hand movement and brain activity from the basic equation for the neural field.

2. THE EXPERIMENTAL OBSERVATIONS

Here we briefly review the results of a recent brain-behavior experiment (Kelso *et al.,* 1998). In this exper-

1053-8119/00 $35.00

iment, subjects were instructed to coordinate the movement of their right (preferred) index finger with a visual metronome at a frequency of 1 Hz in four different task conditions: flexion (extension) synchronized on the metronome beat (F-on and E-on conditions) and flexion (extension) in between consecutive metronome beats (F-off and E-off conditions). Note that these four conditions may be grouped with respect to kinematic characteristics, i.e., direction of the movement (flexion vs extension) or according to coordination mode, i.e., movement in phase or anti-phase with the metronome beats (synchronization vs syncopation).

Measures of finger displacement over time were obtained as pressure changes in an air cushion detected by transducers. During the experiment the magnetic field generated by the ongoing neural activity was measured using a 68-channel full-head magnetometer (CTF, Inc.) at a sampling frequency of 250 Hz. For each condition a total of 100 movement cycles were recorded and the brain signals in each sensor were averaged after artifact removal.

Figure 1 (left) shows the averaged time series of the finger movements for the four task conditions in relation to the metronome for a typical subject. Note that for the on-the-beat conditions the maximum displacement coincides (in phase) with the stimuli, whereas in the off-the-beat conditions the movement is anti-phase with the metronome. Relative phase between the stimulus and the peak of the movement was calculated for each cycle and an average phase for each task condition determined. Figure 1 (middle) shows the relative phase for each cycle plotted in the region from -2π to $+2\pi$ over cycle number. Blue circles indicate cycles which deviate more than $\pm 60°$ from the average value of relative phase and were excluded from further analysis. Figure 1 (right) depicts histograms of the distribution of relative phase. Note that the variance is smaller in the on-the-beat conditions, indicating higher stability for the synchronized movement compared to syncopation (Kelso *et al.*, 1990).

Since the task was to coordinate peak finger flexion or extension with an environmental signal, behavioral and brain data were averaged on a cycle-by-cycle basis with respect to maximum finger displacement for each

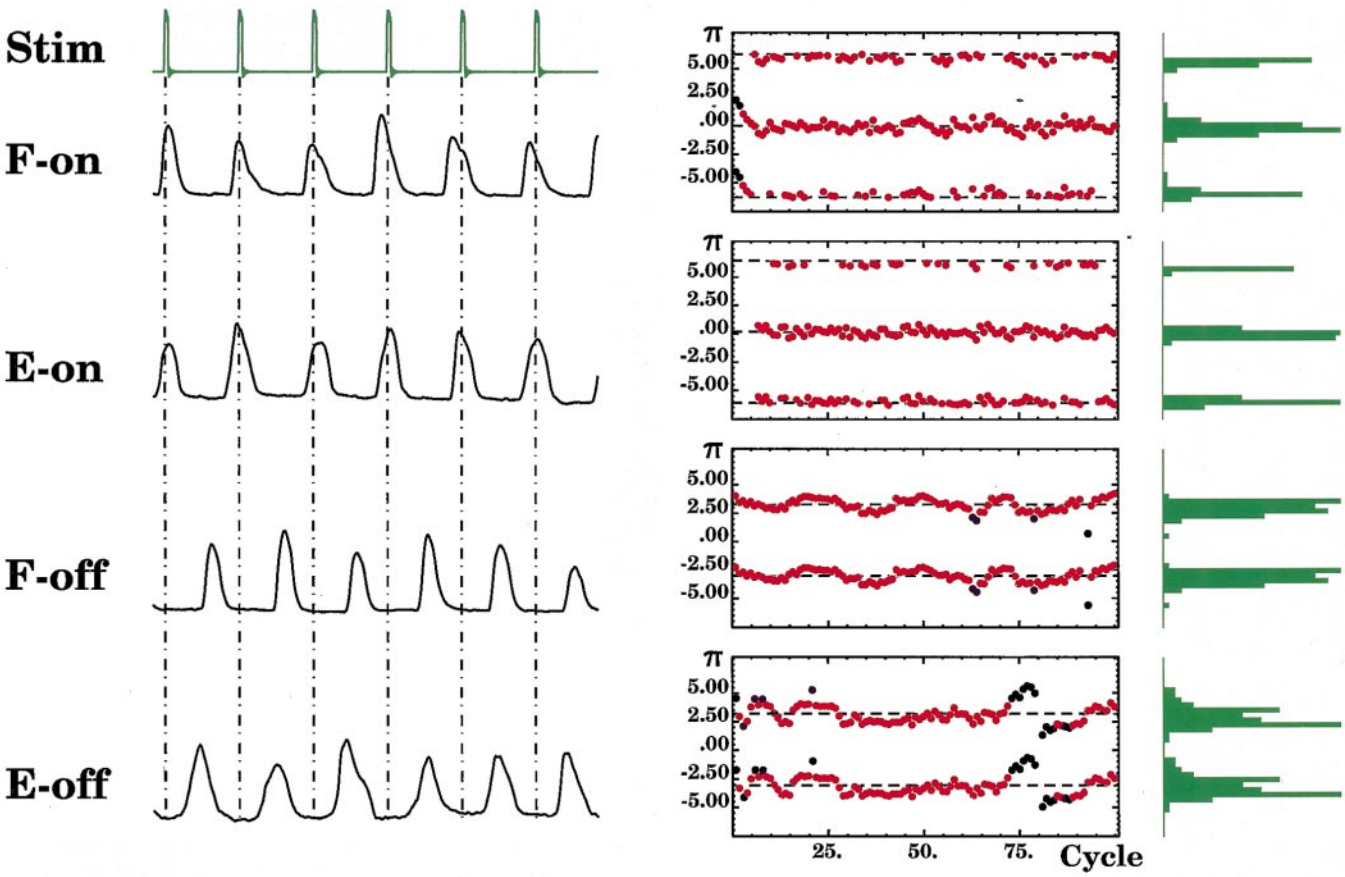

FIG. 1. Relation between stimulus and response for all task conditions. Left: Metronome (green, top) and movement signals for all task conditions. Note that in the on-the-beat conditions the maximum amplitude coincides with the metronome flashes, whereas in the off-the-beat conditions these maxima are in the middle between the flashes. Middle: Relative phase between the stimulus and the maximum of the movement amplitude in a 4π plot. Circles plotted in blue deviate more than 60° from the required phase and were discarded. Right: Histograms of the relative phases. Note that the variance is smaller in the on-the-beat conditions, indicating higher stability.

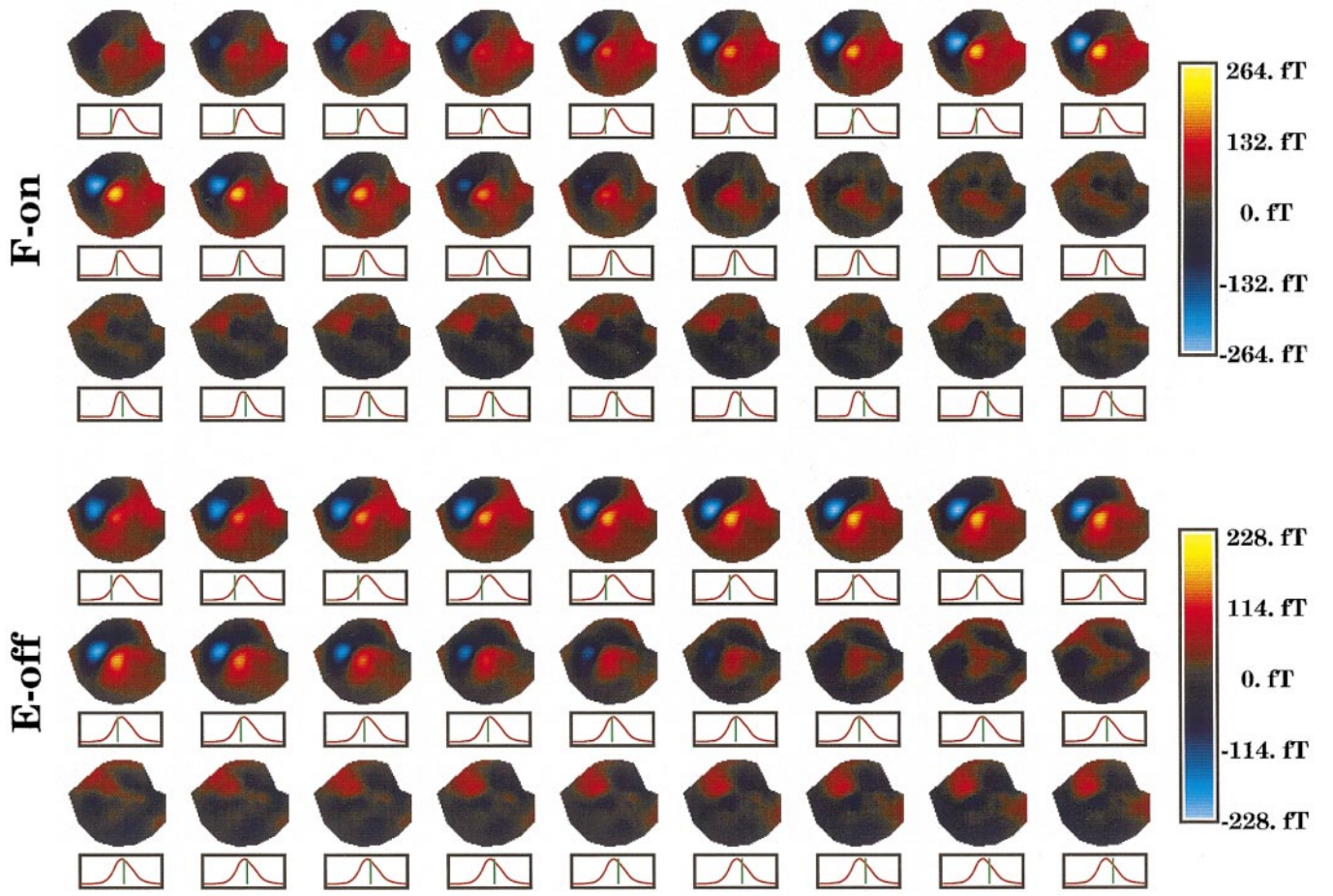

FIG. 2. Topographic maps showing the spatiotemporal dynamics of neural magnetic activity for the flexion-on condition (top three rows) and extension-off condition (bottom three rows). The box below each map shows the movement profile (red) and a green line indicating the location of the map within the cycle. A dipolar pattern appears over the area of left motor cortex, which reaches its maximum amplitude around the inclination point of the left flank of the movement profile. Note that the polarity of this pattern is independent of movement direction.

task condition. Figure 2 shows topographic maps of the temporal evolution of brain activity during the finger movement for the conditions flexion-on and extension-off (the other two conditions were similar). Below each spatial pattern the movement profile (red) is plotted together with a green bar indicating the brain pattern's location within the cycle. Near movement onset a strong dipolar field arises over the left hemisphere. After maximum displacement is reached a dipolar field with reversed polarity and smaller amplitude is visible. Note that these dipolar structures appear to be independent of the direction of movement (flexion vs extension). They also appear to reach their maximum magnitude at the time points of the peak movement velocity, i.e., where the slope of the movement profile is greatest.

In order to illustrate this correlation Fig. 3 shows an overlay of the averaged brain signals from each SQuID with the velocity profile of the movement for the flexion-on condition. Especially inside the highlighted area, where the magnitude of the magnetic field is strong, these curves are almost a perfect match (right yellow circle), likewise if one is multiplied by -1 (left yellow circle). It is evident that a strong correlation (or anti-correlation due to the dipolar nature of magnetic fields) exists between the neural activity and the velocity of the movement, a result of some interest for those who study the neural control of movements (see, e.g., Georgopoulos, 1991, for review).

3. BRIDGE BETWEEN THEORY AND EXPERIMENT: ANALYSIS OF SPATIOTEMPORAL BRAIN SIGNALS

In general, any decomposition of a spatiotemporal pattern $\psi(x, t)$ into spatial modes $\Phi^i(x)$ and corresponding time-dependent amplitudes $\xi_i(t)$ is given by

$$\psi(x, t) = \sum_i \xi_i(t)\Phi^i(x). \quad (1)$$

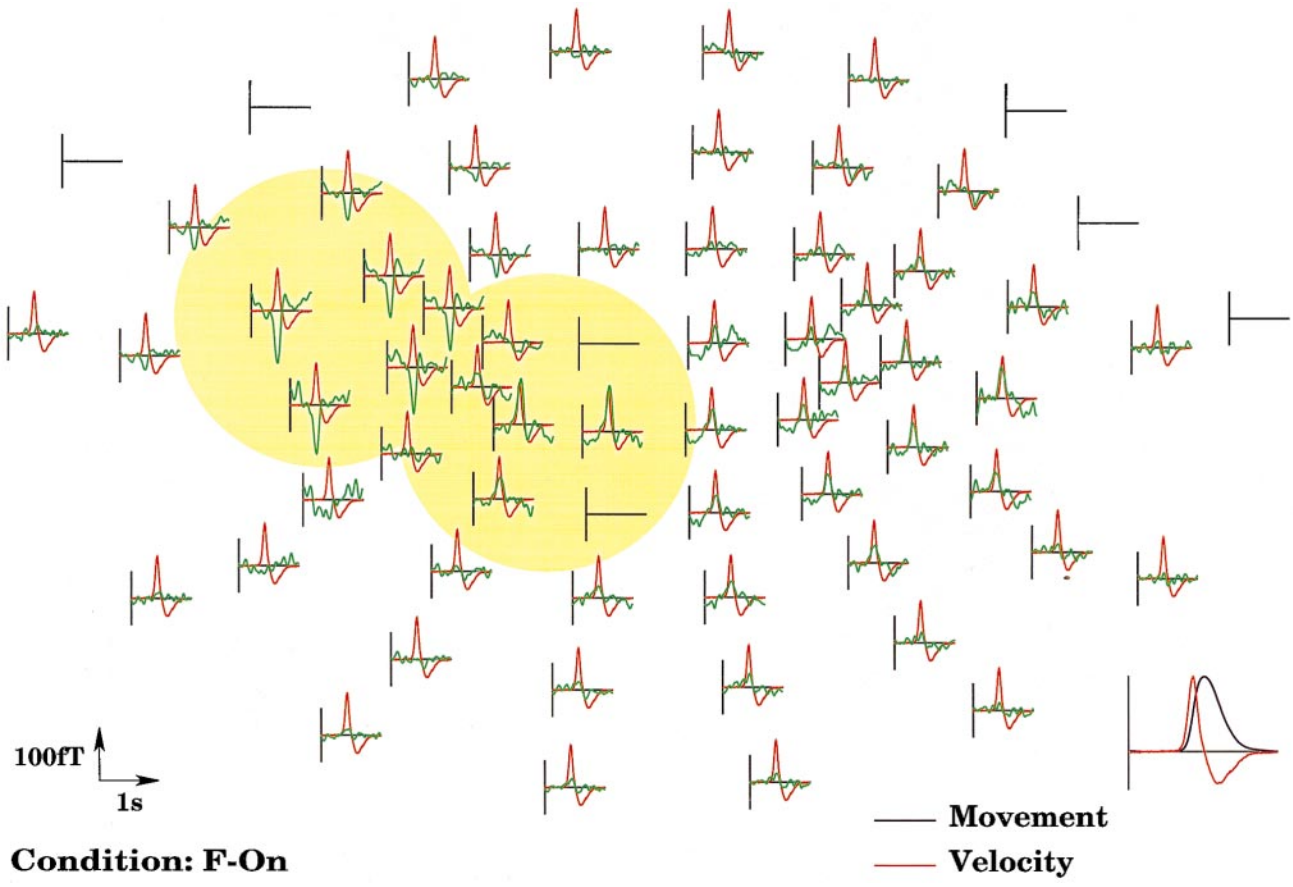

FIG. 3. Overlap between brain signals (green) and movement velocity (red) in single channels. The correlation (or anti-correlation) is extremely high in channels inside the highlighted area. On the bottom right the relation between the movement profile (blue) and movement velocity (red) is shown.

In the discrete case this decomposition reads

$$\psi_k(t) = \sum_i \xi_i(t) v_k^{(i)}, \tag{2}$$

where $\psi_k(t)$ represents the time series at sensor k and $\{\mathbf{v}^{(i)}\}$ a set of basis vectors. Motivated by the strong correlation observed between movement velocity and brain signals we decompose the brain patterns as

$$\psi_k(t) = r(t) v_k^{(1)} + \dot{r}(t) v_k^{(2)}, \tag{3}$$

where $r(t)$ denotes the time series of the finger displacement and $\dot{r}(t)$ the movement velocity. The spatial modes $\mathbf{v}^{(1)}$ and $\mathbf{v}^{(2)}$ are determined by linear regression such that the least-square norm E between the original brain signal and its decomposition (3) is minimized:

$$E = \frac{1}{T} \int_0^T dt \sum_k \{\psi_k(t) - r(t) v_k^{(1)} - \dot{r}(t) v_k^{(2)}\}^2 = \text{Min}. \tag{4}$$

The minimum is found by varying E with respect to vector components $v_j^{(i)}$

$$\frac{\partial E}{\partial v_j^{(1)}} \sim \int_0^T dt \sum_k \{\psi_k(t) - r(t) v_k^{(1)} - \dot{r}(t) v_k^{(2)}\} r(t) = 0 \tag{5}$$

$$\frac{\partial E}{\partial v_j^{(2)}} \sim \int_0^T dt \sum_k \{\psi_k(t) - r(t) v_k^{(1)} - \dot{r}(t) v_k^{(2)}\} \dot{r}(t) = 0. \tag{6}$$

The solution of this linear system of equations readily gives the required spatial modes $\mathbf{v}^{(1)}$ and $\mathbf{v}^{(2)}$. In contrast to modes obtained through procedures like Principal Component Analysis, $\mathbf{v}^{(1)}$ and $\mathbf{v}^{(2)}$ are not necessarily orthogonal. Therefore, a set of adjoint vectors $\mathbf{v}^{(1)+}$ and $\mathbf{v}^{(2)+}$ has to be calculated such that the relation

$$\mathbf{v}^{(i)+} \mathbf{v}^{(j)} = \delta_{ij} \tag{7}$$

is fulfilled (where δ_{ij} represents the Kronecker delta). These modes are obtained by restricting $\mathbf{v}^{(i)+}$ to the subspace defined by $\mathbf{v}^{(1)}$ and $\mathbf{v}^{(2)}$, i.e., writing them in the form

$$\mathbf{v}^{(i)+} = a_{i1}\mathbf{v}^{(1)} + a_{i2}\mathbf{v}^{(2)} \tag{8}$$

and applying relation (7). The time-dependent amplitudes are given by

$$\xi_i(t) = \sum_k v_k^{(i)+}\psi_k(t). \tag{9}$$

Figure 4 shows decompositions of the spatiotemporal brain signal for the four task conditions. For each condition the upper patterns represent the modes $\mathbf{v}^{(1)}$ and $\mathbf{v}^{(1)+}$ corresponding to the finger displacements; the lower patterns $\mathbf{v}^{(2)}$ and $\mathbf{v}^{(2)+}$ correspond to the movement velocity. Plotted on the right for each condition are the time series of the averaged displacement (red, top) and its temporal derivative, the movement velocity (red, bottom). Green curves represent the projections of the original brain signal onto the adjoint vectors, i.e., the time-dependent amplitudes $\xi_1(t)$ and $\xi_2(t)$ for a reconstruction of the signal according to (3). The value of tot is an estimate of the quality of the reconstruction if both modes are used, i.e., the proportion of variance accounted for.

From the spatial patterns $\mathbf{v}^{(1)}$ and $\mathbf{v}^{(2)}$ together with their time-dependent amplitudes $\xi_1(t)$ and $\xi_2(t)$, respectively, the signal at the locations of the sensors can be reconstructed. Figure 5 shows an overlay of the original signal (green) and the reconstruction (red) from the two spatial patterns and their amplitudes. Evidently, most of the spatiotemporal dynamics is reproduced.

4. CONNECTING THEORY AND EXPERIMENT

The most established field theoretical approaches for modeling neural activity are the models by Wilson and Cowan (1972, 1973) and by Nunez (1974,). The Wilson–Cowan model describes the evolution of neural firing rates in space and time, defined on an intracortical space–time scale of 10 ms and millimeters. The Nunez model considers also long-distance contributions of the cortical fiber system and is formulated in terms of synaptic activities which are linearly related to dendritic currents. The latter give rise to the signals observed in EEG and MEG, but can also be mapped onto firing rates (see Jirsa and Haken, 1997, 1996). In recent years these models could be connected and formulated on a macroscopic scale in space and time (i.e.,

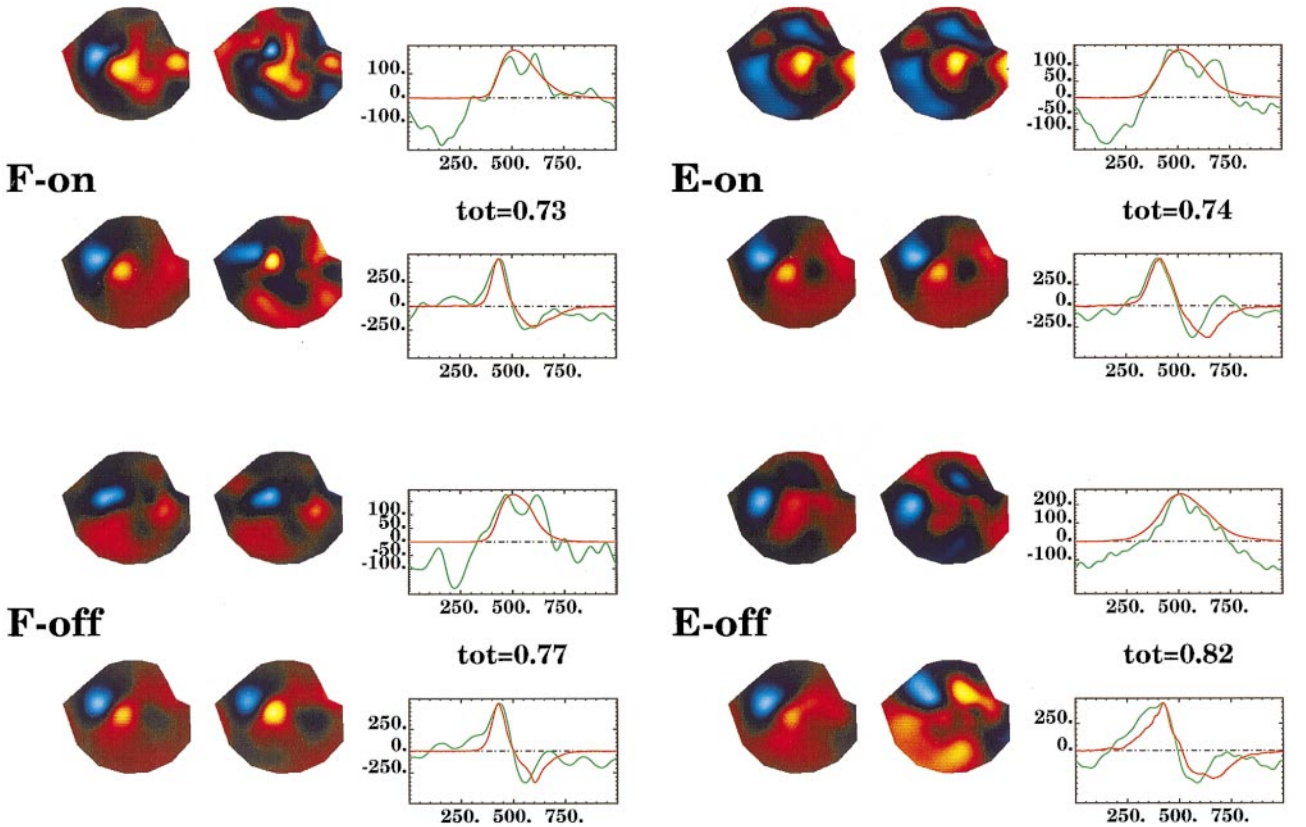

FIG. 4. Biorthogonal decomposition of the brain signal into spatial modes fitting movement and velocity (see text).

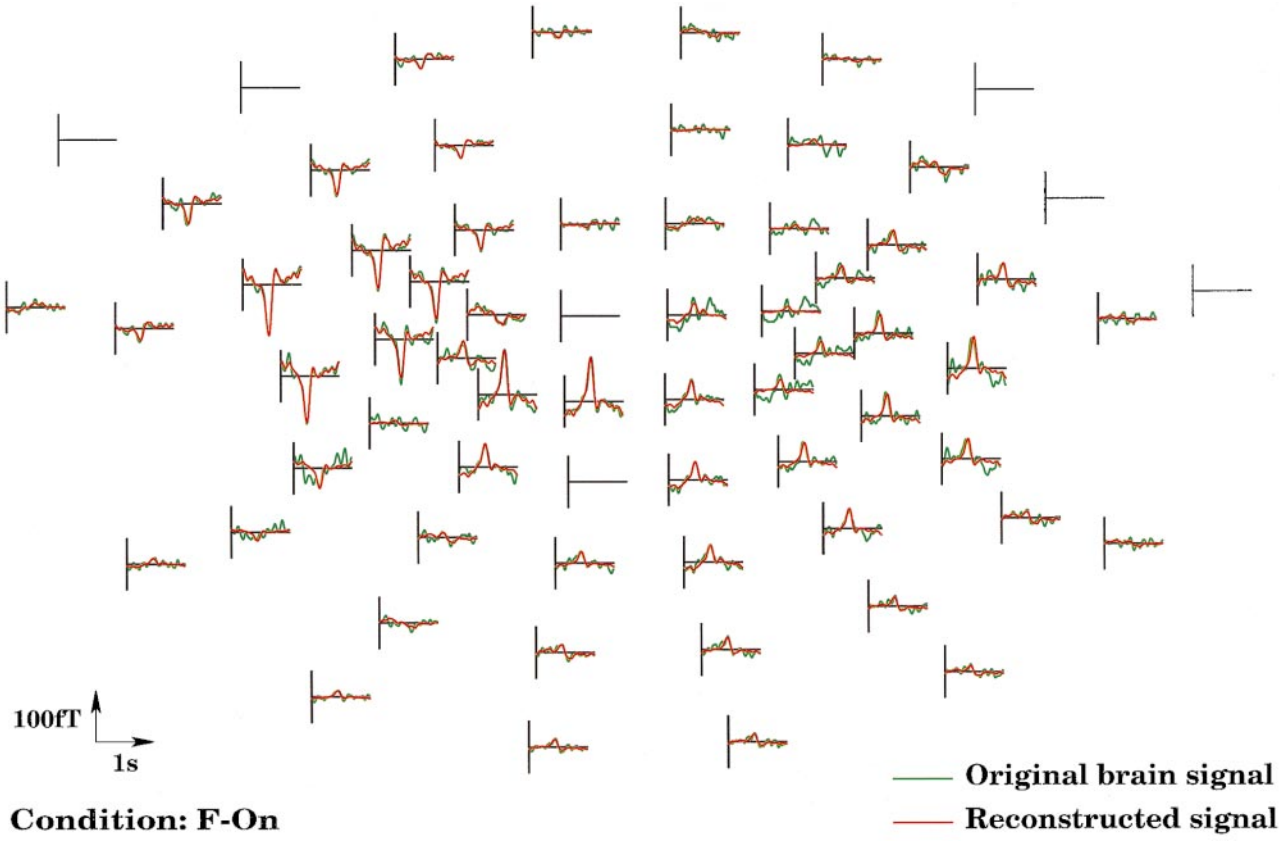

FIG. 5. Reconstruction of brain signals from the two spatial modes $\mathbf{v}^{(1)}$ and $\mathbf{v}^{(2)}$ for the flexion-on condition. Plotted are the original signal in green and the reconstructed signal in red. Note that the reconstruction is very good especially in regions where the amplitude of the brain signal is large.

the scale of centimeters and 100 ms) as a single nonlinear retarded integral equation for the field $\psi(x, t)$ in the neural sheet Γ

$$\psi(x, t) = a \int_{\Gamma} dX\, f(x - X) \cdot S\left[\rho\psi\left(X, t - \frac{|x - X|}{v}\right) + p\left(X, t - \frac{|x - X|}{v}\right)\right]. \tag{10}$$

The neural field $\psi(x, t)$ denotes the relative amplitude of the dendritic currents generated in a neural mass at location x and time t. Its amplitude is relative to an average activity, thus it can acquire positive and negative values. Equation (10) states that the neural activity in the cortical sheet at location x and time t is the weighted sum of activity this location receives from all other locations X and the input units p at X which will be our main concern in later sections. Since activity in the sheet spreads at a finite velocity v it takes the time $|x - X|/v$ to reach the location x from the point X where it originated. The distribution function $f(x - X)$ describes the connection strength between x and X, ρ is the fiber density, and a is the synaptic weight. The sigmoid function S is approximately linear around the origin and saturates for large positive or negative arguments.

Using the method of Green's functions (Jirsa and Haken, 1997) and assuming that the distribution function is given by

$$f(|x - X|) = \frac{1}{2\sigma} e^{|x-X|/\sigma}, \tag{11}$$

i.e., the connectivity falls off exponentially with distance, integral Eq. (10) can be rewritten in one dimension as a nonlinear partial differential equation,

$$\ddot{\psi}(x, t) + \left(\omega_0^2 - v^2 \frac{\partial^2}{\partial x^2}\right)\psi(x, t) + 2\omega_0\dot{\psi}(x, t) = a\left(\omega_0^2 + \omega_0 \frac{\partial}{\partial t}\right) \cdot S[\rho\psi(x, t) + p(x, t)], \tag{12}$$

where $\omega_0 = v/\varsigma$ (see Jirsa and Haken, 1997, 1996, for a detailed derivation). This theory has been applied to a situation in which subjects switch from a syncopated coordination mode to synchronization when the presentation rate of a stimulus is systematically increased (Kelso *et al.*, 1990, 1992). The neural activity reorganizes at the transition point, i.e., the dominating pattern recorded in MEG changes from the shape shown in Fig. 6 bottom left to the one shown on bottom right.

The spatiotemporal dynamics from a numerical integration of (12) is displayed as an x,t plot in Fig. 6, top, with space in the vertical direction and time running horizontally. The input into the neural sheet $p(t)$ shown below the x,t plot is spatially uniform. The initial condition is set to a pattern that corresponds to a slow stimulus frequency which is stable in the "syncopation" mode. When the stimulus rate is increased (as in the real experiment) this pattern becomes unstable and switches to the pattern that corresponds to "synchronization." The dominating patterns from the simulation prior to and after the switch are shown as boxes next to the circles that represent the patterns from the experiment. Notice that shape changes from approximately constant in space to a pattern that has a maximum and a minimum. Second, prior to the transition the amplitude of the constant pattern (blue line in the diagram), oscillating at the same frequency as the stimulus, is dominating. Past the transition the other pattern, which oscillates at twice the stimulus frequency, takes over. This switch in the temporal domain is also observed in the experiment (see for details Fuchs *et al.*, 1992; Kelso *et al.*, 1992; see also Jirsa *et al.*, 1994, for modeling of this effect).

The main point of this paper is to show how the experimental findings presented in section 2 are related to the foregoing theory and how the actual movement profile can be derived from this field theoretical model. In other words, the goal is to derive an equation of the form (3) from the general formulation and relate all dependencies and coefficients to quantities that are accessible from the experimental data. The relation between the internal brain dynamics, sensory inputs, and motor outputs within the theory is handled by functional units, i.e., certain locations or areas in the

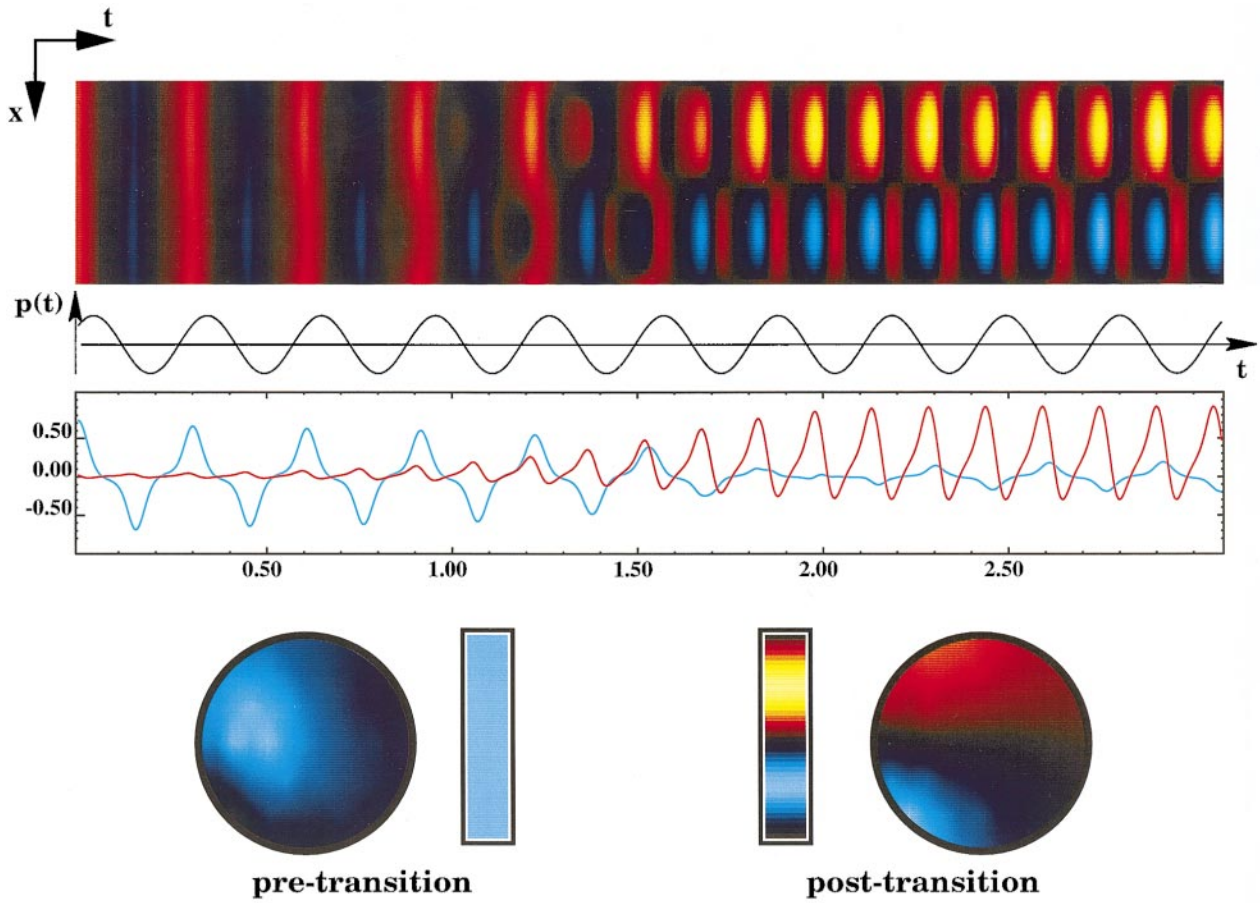

FIG. 6. Reorganization of the spatiotemporal activity at the transition from syncopated to synchronized movement simulated from the field theoretical model. The switch from a spatially constant pattern (blue box, left bottom) and its amplitude oscillating at the stimulus frequency (blue time series) to a pattern with a minimum and maximum (box bottom right) in space oscillating at twice this rate matches the experimental observation (compare text).

cortical sheet. The sum of all inputs constitutes the function $p(x, t)$ in (12). An output signal is created as the weighted sum of activity over the corresponding output areas. The following two subsections describe how these units are represented in their general form and how they can be simplified under certain assumptions.

4.1. Functional Input Units

Peripheral signals, such as in proprioceptive or cutaneous feedback, generate activity in receptors that is typically conveyed via the brain stem to higher areas of the brain, in particular the neocortex. These afferent signals excite neocortical neuron populations at specific locations and cause them to fire. Obviously, the input-response mechanism between the periphery and the excited neuron populations is complex and may involve higher order contributions from memory and internal feedback loops as well as depending on the overall task context. The goal here, however, is not to identify individual contributions to the input-response mechanism but to define a compact mapping of the peripheral signal to the time course of the firing rate of the neural population that receives afferent excitation. The latter is called a functional input unit $p(x, t)$ and can be formally expressed as

$$p(x, t) = \int_{t_0}^{t} F(x, t, \tau) N^i(r_j(\tau))\, d\tau, \qquad (13)$$

where the integral kernel $F(x, t, \tau)$ defines its spatial localization in the cortical sheet and a temporal convolution. $N^i(r_j(\tau))$ (where i denotes input) is a nonlinear function. We make two assumptions:

1. There is a translational invariance in the temporal domain, i.e., the integral kernel depends only on the difference $t - \tau$, and
2. the integral kernel factorizes in space and time,

$$F(x, t - \tau) = \beta^i(x) f(t - \tau), \qquad (14)$$

which means that we neglect spatiotemporal input phenomena such as traveling waves within a functional unit.

Then (13) can be written as

$$p(x, t) = \beta^i(x) \int_{t_0}^{t} f(t - \tau) N^i(r_j(\tau))\, d\tau. \qquad (15)$$

4.2. Functional Output Units

Similarly, an output signal $r(t)$ to the periphery is related to the cortical activity $\psi(x, t)$ via

$$r(t) = \int_{\Gamma} \int_{t_0}^{t} G(x, t, \tau) N^o(\psi(x, \tau))\, d\tau\, dx, \qquad (16)$$

where the integration in space, denoted by Γ, takes the sum of all neural activity on the cortical sheet related to $r(t)$ by the integral kernel G. Under the same assumptions as in section 4.1 we rewrite the integral kernel as

$$G(x, t, \tau) = \beta^o(x) g(t - \tau), \qquad (17)$$

where $\beta^o(x)$ defines the spatial localization of the functional output unit, $g(t - \tau)$ defines the temporal convolution, and o stands for output. We obtain

$$r(t) = \int_{\Gamma} \beta^o(x)\, dx \int_{t_0}^{t} g(t - \tau) N^o(\psi(x, \tau))\, d\tau. \qquad (18)$$

Now we relate the spatial localizations $\beta^{i,o}(x)$ and the temporal transfer functions $f(t - \tau)$, $g(t - \tau)$ to the experimental data described in section 2.

4.3. Relation between Brain Theory and Movement

In section 2 we saw that the two signals, $r_j(t)$, the finger movement, and $\psi(x, t)$, the brain activity, both oscillate with the same frequency. A simple Fourier decomposition shows that the nonlinear functions $N^{i,o}$ can be approximated by their linear contributions. This is not trivial as shown in the previous section in which in the synchronization mode the brain signal oscillates at twice the stimulus rate (which means that nonlinearities need to be included). On the large spatiotemporal scale obtainable by EEG/MEG measurements the input and output localizations are not readily distinguishable, hence we approximate them as

$$\beta_j^i(x) \approx \beta_j^o(x) = \beta(x), \qquad (19)$$

and drop the index j since we will be concerned with one spatial function only. Now (18) can be written in the form

$$r(t) = \int_{\Gamma} \beta(x)\, dx \int_{t_0}^{t} g(t - \tau) \psi(x, \tau)\, d\tau. \qquad (20)$$

By integrating over space which gives the total input into the cortical sheet at time t, (15) becomes

$$p(t) = \int_\Gamma p(x,\, t)\, dx = \int_\Gamma \beta(x)\, dx \int_{t_0}^{t} f(t-\tau) r(\tau)\, d\tau. \tag{21}$$

Inserting (20) into (21) we obtain the general relation between the motor event $r(t)$ and the spatiotemporal neural activity $\psi(x, t)$,

$$\int_{t_0}^{t} f(t-\tau) r(\tau)\, d\tau = \int_{t_0}^{t} f(t-\tau)\, d\tau \cdot \int_{t_0}^{\tau} g(\tau-\tau')\, d\tau' \int_\Gamma \beta(x)\psi(x,\, \tau')\, dx. \tag{22}$$

Now we expand $r(\tau)$ on the l.h.s. of (22) into a Taylor series around t,

$$c_0 r(t) + c_1 \dot{r}(t) + c_2 \ddot{r}(t) + \cdots = \text{r.h.s.}, \tag{23}$$

where the expansion coefficients c_n are given by

$$c_n = \int_{t_0}^{t} f(t-\tau)\, \frac{(\tau - t)^n}{n!}\, d\tau. \tag{24}$$

From the experimental data we know that the spatiotemporal neural activity can be approximated by two spatial patterns multiplied by the time course of the movement amplitude and velocity

$$\psi(x,\, t) \approx \beta^{(0)}(x) r(t) + \beta^{(1)}(x) \dot{r}(t). \tag{25}$$

Multiplying (25) by a spatial weight function $\beta(x)$ and integrating over space yields

$$r(t) \int_\Gamma \beta(x)\beta^{(0)}(x)\, dx + \dot{r}(t) \int_\Gamma \beta(x)\beta^{(1)}(x)\, dx \approx \int_\Gamma \beta(x)\psi(x,\, t)\, dx, \tag{26}$$

which approximates an ordinary differential equation of a driven overdamped harmonic oscillator of the form

$$a_0 r(t) + a_1 \dot{r}(t) = h(t). \tag{27}$$

Comparing (26) with (23) we see that the temporal convolutions on the r.h.s. of (22) must be equal to the identity operator and that the coefficients c_n have to vanish for $n \geq 2$. This means that we do not need to take into account higher order derivatives, such as acceleration or jerk (Flash and Hogan, 1985), that have been postulated to be significant for the organization of movement.

We now identify the spatial function $\beta(x)$, which represents the input–output unit in the theory with the pattern $\mathbf{v}^{(2)}$, the dominating mode in the experiment. Using a discrete notation and assuming that $\mathbf{v}^{(2)}$ is normalized in the way $\mathbf{v}^{(2)}\mathbf{v}^{(2)} = 1$, Eq. (26) reads

$$\dot{r}(t) + \mathbf{v}^{(2)}\mathbf{v}^{(1)} r(t) = \sum_j v_j^{(2)} \psi_j(t), \tag{28}$$

where $\psi_j(t)$ represents the time series recorded in sensor j. This determines all quantities in (27), namely

$$a_0 = \mathbf{v}^{(2)}\mathbf{v}^{(1)}, \quad a_1 = 1, \quad \text{and} \quad h(t) = \sum_j v_j^{(2)} \psi_j(t), \tag{29}$$

which can be easily solved. The solution for large t is given by

$$r(t) = \kappa \int_{t_0}^{t} h(\tau) e^{-a_0(t-\tau)}\, d\tau. \tag{30}$$

The effects of the operation on the r.h.s. of (30) are shown in Fig. 7. In the top row left the input function $h(t)$ is a sine function plotted in red. The resulting function $r(t)$ (in blue) is shifted by a quarter of a period representing a minus cosine or the sine function's antiderivative. In top right noise is added to the input. Nevertheless, the output is still smooth due to the integration in time. In the bottom row the derivative from the flexion-on movement amplitude is used as input (red). The output is a smooth movement profile even if noise is added to the input (bottom left).

Equation (30) together with (29) expresses the time series of the movement in terms of the brain activity. There is only one free scaling parameter κ relating the units in which the movement and the magnetic field are measured. All other terms are well defined and can be determined from the experimental data. Figure 8 shows the reconstruction of the movement profile from the underlying neural activity according to (30) for all task conditions. Note that the reconstructed movement profile fits the experimentally observed movement particularly well in the active phase of the movement represented by its positive flank. Discrepancies mainly occur after peak displacement and are probably due to the sensory feedback which is not accounted for in the present formulation.

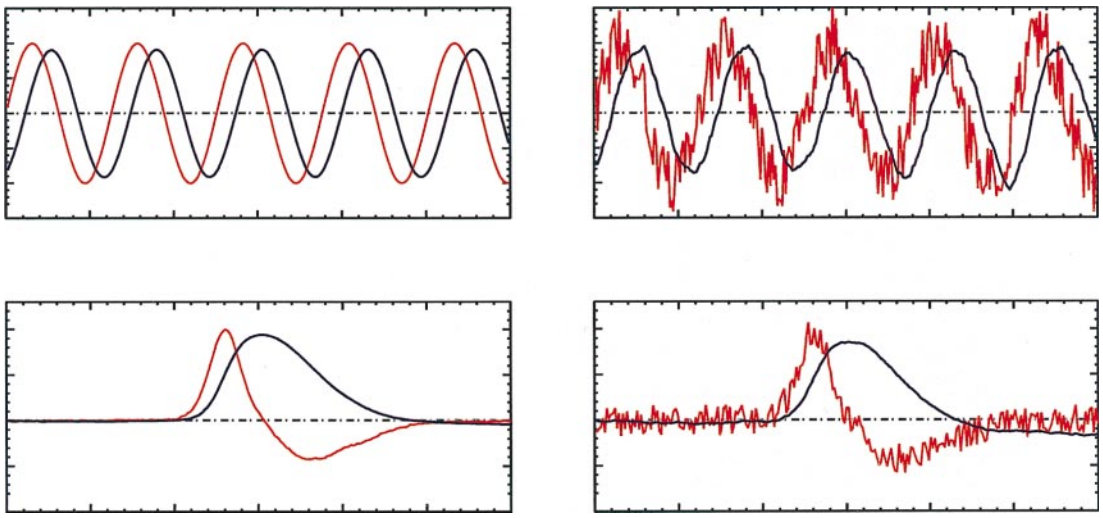

FIG. 7. Effect of the temporal integration on the r.h.s. of Eq. (30) on different input functions. Top left: The input $h(t)$ is a sine function plotted in red, the output $r(t)$ is shifted by a quarter of a period representing the anti-derivative, a minus cosine. Top right: Noise is added to the input signal—the output is still a smooth. Bottom: The input is the derivative of the movement amplitude from the flexion-on condition (red). The output is a smooth movement profile (blue) even if the input is noisy.

Finally, from (24) and (30) we can find an explicit form of the transfer functions $f(t-\tau)$ and $g(t-\tau)$ for the input and output units, respectively:

$$f(t-\tau) = \left[c_0 + \frac{\partial}{\partial t}\right]\delta(t-\tau) \qquad \text{and} \qquad g(t-\tau) = e^{a_0(t-\tau)}. \tag{31}$$

This closes the loop between the quantities that are observed experimentally and the functions used in the theoretical modeling in a self-consistent fashion.

5. SUMMARY AND CONCLUSION

How are biological events such as a finger movement related to or represented by ongoing activity in the brain? In recent experimental work, summarized here, we have established that a close relation holds between the velocity of the movement and the MEG signal recorded over certain areas of sensorimotor cortex (Kelso *et al.*, 1998). Under the theoretical assumption that the experimentally observed dipolar pattern represents the functional input and output activity of the cortical sheet we were able to derive the observed time course of the movement produced. As a result, the amplitude of the movement at a certain time is given as an integration over space and time and may be characterized as an overdamped oscillator driven by the amplitude of the dipolar brain pattern.

Our observations and theory may speak to one of the reigning hypotheses about how the brain controls voluntary movements: The mass spring (Bizzi *et al.*, 1991; Feldman, 1966; Kelso, 1977; Polit and Bizzi, 1978) or, in its new guise, the equilibrium point hypothesis. Recent tests of the equilibrium hypothesis are based on

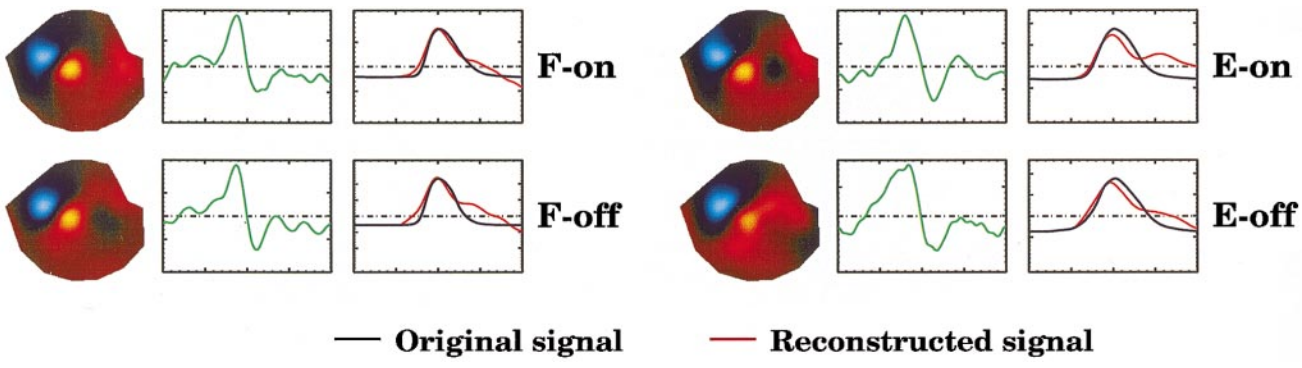

FIG. 8. Reconstruction of movement profile from brain activity. For all four task conditions on the left the spatial pattern corresponding to movement velocity is shown. The green curves are their time-dependent amplitudes, the function $h(t)$ in (30). The right boxes for each condition show overlays of the actual movement profile in blue and the reconstruction, the function $r(t)$ in (30) in red.

peripheral measures of stiffness obtained during arm movement (Gomi and Kawato, 1996) and subsequent inferences regarding the form of the signal sent by the brain. Direct measures of brain activity obtained in our work show that the brain does indeed generate signals that reproduce the actual movement trajectory independent of direction. The present theory shows how this neural signal may drive the finger, the intrinsic dynamics of which have been shown to correspond to a damped mass spring system (Kelso and Holt, 1980). An approach complementary to ours has been taken by Shidara *et al.* (1993), who show how the complex firing of Purkinje cells in the cerebellum can be reconstructed by inverse dynamics methods that use position, velocity, and acceleration of the eye (see also Wolpert *et al.*, 1995). Though the mechanisms and the modeling strategy are different, both approaches suggest that brain and behavior can be captured in the common currency of dynamics.

In our work the relation between the experimentally observed quantities, i.e., the magnetic field picked up by the sensors, and the spatial and temporal transfer functions used in the model is unique and all parameters (except the scaling between amplitudes of the brain signal and the movement) are determined. In other words no free parameters are available that could influence the time course of the movements in the various task conditions as they are predicted by the model. This close connection between theory and experiment supports our contention that the global dynamical properties of the brain may be understood, theoretically modeled, and linked to human behavior.

ACKNOWLEDGMENTS

This research was supported by NIMH (Neurosciences Research Branch) Grants MH42900 and KO5 MH01386 to J.A.S.K. and the Human Frontier Science Program. We thank Tom Holroyd for his help during the data collection.

REFERENCES

Bizzi, E., Muss-Ivaldi, F. A., and Giszter, S. 1991. Computations underlying the execution of movement: A biological perspective. *Science* **253:**287–291.

Feldman, A. G. 1966. Functional tuning of the nervous system with control of movement or maintenance of a steady posture. III. Mechanographic analysis of execution by man of the simplest motor tasks. *Biophysics* **11:**766–775.

Flash, T., and Hogan, N. 1985. The coordination of arm movements: An experimentally confirmed mathematical model. *J. Neurosci.* **5:**1688–1703.

Fuchs, A., Kelso, J. A. S., and Haken, H. 1992. Phase transitions in the human brain: Spatial mode dynamics. *Int. J. Bifurc. Chaos* **2:**917–939.

Georgopoulos, A. P. 1991. Higher order motor control. *Annu. Rev. Neurosci.* **14:**361–377.

Gomi, H., and Kawato, M. 1996. Equilibrium-point control hypothesis examined by measured arm stiffness during multijoint movement. *Science* **272:**117–120.

Haken, H. 1996. *Principles of Brain Functioning.* Springer, Berlin.

Jirsa, V. K., Friedrich, R., Haken, H., and Kelso, J. A. S. 1994. A theoretical model of phase transitions in the human brain. *Biol. Cybernet.* **71:**27–35.

Jirsa, V. K., Friedrich, R., and Haken, H. 1995. Reconstruction of the spatio-temporal dynamics of a human magnetoencephalogram. *Physica* **D89:**100–122.

Jirsa, V. K., and Haken, H. 1996. Field theory of electromagnetic brain activity. *Phys. Rev. Lett.* **77:**960–963.

Jirsa, V. K., and Haken, H. 1997. A derivation of a macroscopic field theory of the brain from the quasi-microscopic neural dynamics. *Physica* **D99:**503–526.

Jirsa, V. K., Fuchs, A., and Kelso, J. A. S. 1998. Connecting cortical and behavioral dynamics: Bimanual coordination. *Neural Comput.* **10:**2019–2045.

Kelso, J. A. S. 1977. Motor control mechanism underlying human movement reproduction. *J. Exp. Psychol. Hum. Percept. Perform.* **3:**529–543.

Kelso, J. A. S. 1984. Phase transitions and critical behavior in human bimanual coordination. *Am. J. Physiol.* **15:**R1000–R1004.

Kelso, J. A. S. 1995. *Dynamic Patterns. The Self-Organization of Brain and Behavior.* MIT Press, Cambridge, MA.

Kelso, J. A. S., and Holt, K. G. 1980. Exploring a vibratory systems analysis of human movement production. *J. Neurophysiol.* **43:** 1183–1196.

Kelso, J. A. S., DelColle, J. D., and Schöner, G. 1990. Action-perception as a pattern formation process. In *Attention and Performance XIII* (M. Jeannerod, Ed.), pp. 139–169, Erlbaum, Hillsdale, NJ.

Kelso, J. A. S., Bressler, S. L., DeGuzman, G. C., Ding, M., Fuchs, A., and Holroyd, T. 1992. A phase transition in human brain and behavior. *Phys. Lett.* **A169:**134–144.

Kelso, J. A. S., Fuchs, A., Lancaster, R., Holroyd, T., Cheyne, D., and Weinberg, H. 1998. Dynamic cortical activity in the human brain reveals motor equivalence. *Nature* **23:**814–818.

Miller, R. 1987. Representation of brief temporal patterns, Hebbian synapses, and the left-hemisphere dominance for phoneme recognition. *Psychobiology* **15:**241–247.

Nunez, P. L. 1974. The brain wave equation: A model for the EEG. *Math. Biosci.* **21:**279–297.

Nunez, P. L. 1995. *Neocortical Dynamics and Human EEG Rhythms.* Oxford Univ. Press, Oxford.

Polit, A., and Bizzi, E. 1978. Process controlling arm movements in monkeys. *Science* **201:**1235–1237.

Shidara, M., Kawato, K., Gomi, H., and Kawato, M. 1983. Inverse-dynamics models eye movement control by Purkinje cells in the cerebellum. *Nature* **365:**50–52.

Wallenstein, G. V., Kelso, J. A. S., and Bressler, S. L. 1995. Phase transitions in spatiotemporal patterns of brain activity and behavior. *Physica* **D84:**626–634.

Wilson, H. R., and Cowan, J. D. 1972. Excitatory and inhibitory interactions in localized populations of model neurons. *Biophys. J.* **12:**1–24.

Wilson, H. R., and Cowan, J. D. 1973. A mathematical theory of the functional dynamics of cortical and thalamic nervous tissue. *Kybernetik* **13:**55–80.

Wolpert, D., Ghahramani, Z., and Jordan, M. 1995. An internal model for sensorimotor integration. *Science* **269:**1880–1882.